Experimental energy dispersions for valence and conduction bands of iridium

J. F. van der Veen, F. J. Himpsel, and D. E. Eastman

IBM Thomas J. Watson Research Center, Yorktown Heights, New York 10598

(Received 9 May 1980)

Using angle-resolved photoemission with synchrotron radiation, we have determined the energy-versus-momentum dispersion relations $E(\vec{k})$ for the valence bands of Ir along the $\Gamma\Lambda L$ and $\Gamma\Delta X$ symmetry directions. This has been achieved by measuring $h\nu$-dependent normal emission spectra from Ir(111) and metastable unreconstructed Ir(100) (1×1) surfaces. Conduction-band critical points at Γ, X, and L are seen as structures in the angle-resolved energy spectrum of secondary electrons. Semiempirical final bands were used to obtain E vs k energy dispersions of the initial bands. A strong resonance was observed for direct transitions at Γ from the upper d bands ($E = -1.04$ eV relative to the Fermi level E_F) to an sp-like final-state band at $E = +19.5$ eV. The lower spin-orbit-split d band ($E = -3.18$ and -4.07 eV at Γ) couples strongly to both a sp-like final-state band and flat f-like final-state band (located at $E \simeq +15$ eV near Γ). Experimental energy bands are compared with Fermi-surface data and a relativistic-augmented-plane-wave band-structure calculation by Andersen. Surface umklapp scattering is shown to be important for bulk-band emission from the (5×1) reconstructed Ir(100) surface.

I. INTRODUCTION

Angle-resolved photoelectron spectroscopy (ARPES) has been successfully applied to the determination of bulk energy-band dispersions $E(\vec{k})$ for the noble metals and a number of nearly filled $3d$ and $4d$ transition metals. In this paper, we report ARPES studies of the band dispersions $E(\vec{k})$ of Ir, a $5d$ transition metal with nearly filled d bands which has interesting physical properties, e.g., as a catalyst. To date, most information concerning the electronic structure of Ir has been obtained via theoretical studies. An *ab initio* relativistic-augmented-plane-wave (RAPW) method has been used by Andersen[1] to obtain energy eigenvalues of bands at high symmetry points of the Brillouin zone. A similar method has been used by Arbman and Hörnfelt[2] to calculate energy dispersions $E(\vec{k})$ along high-symmetry directions. Smith[3] employed an interpolation scheme with empirically adjusted parameters to calculate energy-band dispersions for various $5d$ and $4d$ transition metals. Subsequently no new band-structure calculations have been performed for Ir of the sort recently completed for Pd (Ref. 4) and Au.[5] Experimentally, indirect information concerning electronic states near the L point in Ir has been provided by optical data and angle-integrated photoemission spectra.[6,7,29] de Haas–van Alphen measurements of Fermi-surface dimensions have been performed by Grodski *et al.*[8] and Hörnfelt *et al.*[9]

In this paper, angle-resolved photoemission spectroscopy has been used to determine E vs $\vec{k}$ dispersions of Ir valence bands along the $\Gamma\Lambda L$ and $\Gamma\Delta X$ symmetry directions as well as critical points of empty

conduction bands. This has been achieved by taking photon-energy dependent photoemission spectra for normal emission from Ir(111) and metastable Ir(100) (1×1) surfaces. As previously reported for Cu,[10] Ni,[11] Pd,[12] and Au,[13] the photoemission data from Ir can be successfully interpreted in terms of a three step model,[14] i.e., with direct energy- and momentum-conserving transitions between initial and final states of the photoexcitation process followed by transport to the surface and transmission through the surface.

For unreconstructed surfaces such as Ir(111) and metastable Ir(100) (1×1) the component of crystal momentum $\vec{k}$ parallel to the surface $(\vec{k}_\parallel)$ is zero in normal emission, since the reduced $\vec{k}_\parallel$ is conserved. As previously reported,[11,12] the perpendicular momentum component $k_\perp$ (which cannot be directly measured) for observed interband transitions was determined via the final-state band dispersions $E_f(k_\perp)$. Lacking a theoretical calculation of final energy bands higher than 13 eV above E_F, we have used experimentally determined critical points for these conduction bands at Γ, X, and L and interpolated between these points by shifting and scaling calculated bands for Au.[5] The initial-state momentum $k_\perp$ is then determined by assuming a direct transition to the semiempirical final band of final energy $E_f = h\nu + E_i$, where $h\nu$ is the photon energy and E_i is the initial energy relative to the Fermi energy E_F. This procedure gives reasonably accurate values of $k_\perp$ (typically $\lesssim 10\%$ of the Brillouin-zone boundary momentum) because the final-state bands are generally quite steep compared to the initial bands.

Apart from its usefulness in determining experi-

mental band dispersions $E(\vec{k})$, which are important for understanding many physical properties and of interest for band-structure calculations, a photoemission study of Ir offers a unique opportunity to assess the importance of "surface umklapp" scattering for bulk band emission from reconstructed surfaces.[15] Namely, the clean Ir(100) surface can be prepared in a stable (5 × 1) reconstructed or in a metastable unreconstructed (1 × 1) phase.[16] This remarkable property that the Ir(100) surface has in common with Pt (100) (Ref. 17) and Au (100) (Ref. 18) surface[5] allows us to study surface scattering effects such as elastic scattering of photoelectrons by the extra (5 × 1) surface lattice vectors of the reconstructed Ir(100) (5 × 1) surface.

The paper is organized as follows: Experimental measurement and surface preparation techniques are described in Sec. II. Section III presents experimental results for normal emission from Ir(111) and Ir(100) (1 × 1). In Sec. IV we summarize our experimental band dispersions $E(\vec{k})$ and compare with available band-structure calculations and Fermi-surface data. Photoemission spectra from the (5 × 1)—reconstructed Ir(100) surface and the importance of surface umklapp processes are discussed in Sec. V.

II. EXPERIMENTAL

Data were taken with a two-dimensional display-type electron spectrometer[19] using synchrotron radiation at the Synchrotron Center of the University of Wisconsin, Madison. This spectrometer combines an ellipsoidal reflection mirror low-pass filter with a retarding grid high-pass filter to achieve a band pass energy analyzer (energy resolution of 0.15 eV) while accepting a full 86° cone of emission angles (1.8 sr). An angle resolving detector selects electrons emitted within this cone and was used with an angular resolution of 6° (full angle). A toroidal grating monochromator was used for photon energies in the range $8 \leq h\nu \leq 30$ eV for this study.

Clean Ir(100) (5 × 1) and Ir(111) surfaces were prepared by sputter-cleaning and repeated cycles of heating in oxygen at 1300 K and flashing *in vacuo* to 1500 K. The surfaces were characterized *in situ* by low-energy electron diffraction (LEED) and Auger electron spectroscopy. The clean metastable Ir(100) (1 × 1) structure was prepared by following the prescription given in Ref. 16. In brief, the Ir(100) (5 × 1) surface was exposed to 30–80 L (1 L = 10⁻⁶ Torr sec) of oxygen (10–25 min at 5 × 10⁻⁸ Torr until saturation coverage was reached). The LEED pattern then showed a faint (2 × 1) structure. The oxygen was subsequently removed by exposing the surface to ~ 60 L of H_2, which yields a streaked (1 × 1) LEED pattern. As for Pt,[20,21] hydrogen reacts readily with adsorbed oxygen at room temperature. The ex-

cess hydrogen on the Ir(100) (1 × 1) surface was removed by mild heating (~ 430 K), resulting in a sharp (1 × 1) LEED pattern. Heating the metastable Ir(100) (1 × 1) sample to a temperature of ~ 800 K for a few seconds was sufficient to restore the stable Ir(100) (5 × 1) structure.
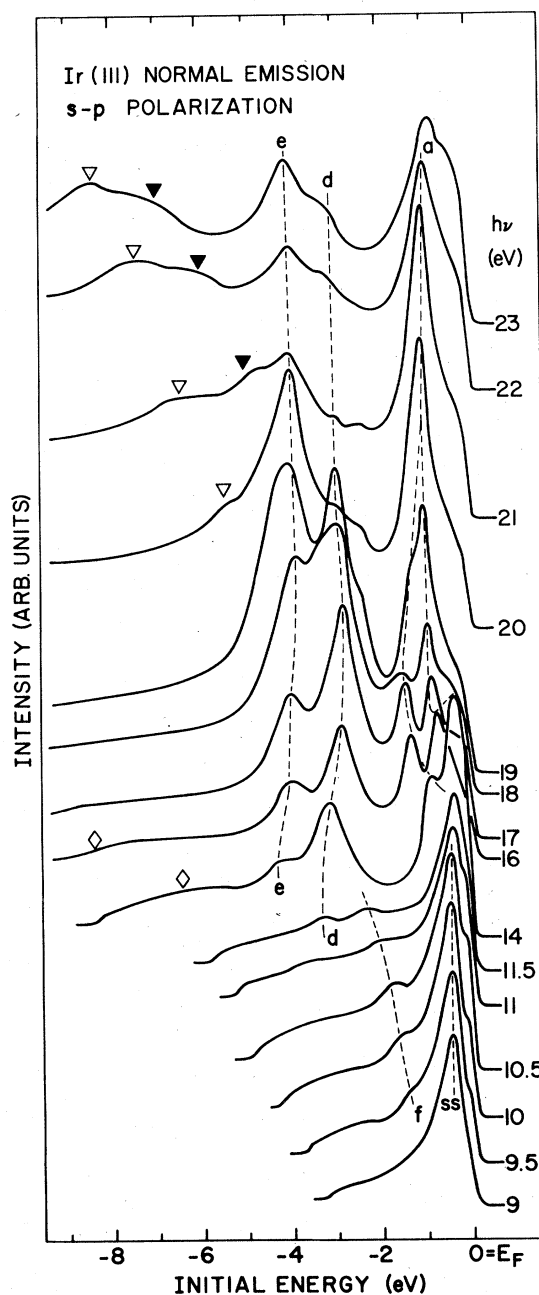
FIG. 1. Normal emission AREDC's from Ir(111). Peaks labeled *a*, *d*, *e*, and *f* are due to bulk interband transitions, peak *ss* marks a surface-state emission feature. Triangular- and diamond-shaped symbols indicate structures in the secondary electron distribution.

III. PHOTOEMISSION FROM Ir(111)
AND Ir(100) (1 × 1)

Angle-resolved electron-energy-distribution curves (AREDC) have been measured in normal emission from Ir(111) and Ir(100) (1 × 1) using 60% p-polarized and pure s-polarized radiation, respectively (Figs. 1 and 2). Initial energies are referred to the experimental Fermi level E_F (accuracy ± 0.05 eV).
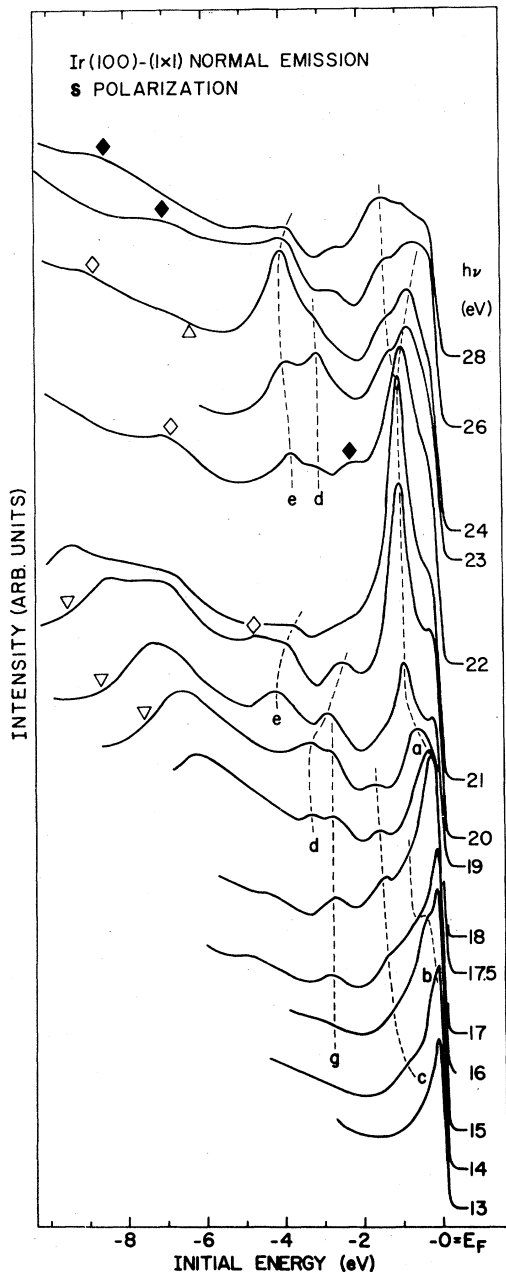
FIG. 2. Normal emission AREDC's from Ir(100) (1 × 1). Symbols are as in Fig. 1.

As general features in the spectra we note (i) dominant peaks, labeled a, b, c, d, e, and f which all disperse with photon energy (or, equivalently, with $k_\perp$) and which can be attributed to direct bulk interband transitions. (ii) Peak g in Fig. 2 is stationary with photon energy and reflects a critical point in the Ir valence-band density of states. (iii) Peak ss in Fig. 1 dominates the normal emission spectra from Ir(111) at low photon energies ($8 < h\nu < 11.5$ eV). It does not disperse with $h\nu$ and is sensitive to gas adsorption. This feature, which is strongly peaked around normal emission, will be shown to lie in a s-p bulk band gap and is due to surface state emission. (iv) Spectral structures in the secondary electron-energy distribution, marked by triangular and diamond-shaped symbols in Figs. 1 and 2. These structures correspond to critical points of empty conduction bands, as we will discuss next.

A. Conduction-band critical points

The low kinetic energy portions of the normal emission AREDC's in Figs. 1 and 2 are due to secondary electron emission (inelastically scattered electrons). These portions of the spectra are expected to reflect structure in the one-dimensional density of final states along $\Gamma\Lambda L$ and $\Gamma\Delta X$ symmetry directions, respectively.[12,22] The open triangles (∇) in Fig. 2 denote such a structure, which is seen as a change in slope in the secondary electron spectrum from Ir(100) (1 × 1). This spectral structure is due to a decrease in escape depth as the final-state energy approaches from above the minimum energy of the free-electron-like sp band at the X_6^+ point which has a final-state energy of 10.5 eV. [High-symmetry points for final bands are given the same double group symmetry labels as corresponding calculated bands for Au (Refs. 5 and 23).] Final states in the sp band gap below the X_{6+} point are evanescent in the bulk, resulting in decreased escape depths and a corresponding reduction in the secondary electron yield below the X_{6+} point. A similar, less pronounced structure appears in the spectra for Ir(111) at a final energy of $E_f = 7.6$ eV [indicated by open diamonds ($\diamond$) in Fig. 1]. This structure marks the minimum of the sp band at L_{6+}. At higher photon energies, the maximum of the sp-like final band at Γ_7^- is seen as a weak structure at $E_f = 19.5$ eV [closed diamonds ($\blacklozenge$) in Fig. 2, not shown in Fig. 1].

A double-peaked structure in the normal emission spectra from Ir(111) is observed at final energies of 14.5 and 16.0 eV [open (∇) and closed ($\blacktriangledown$) triangles in Fig. 1]. This structure originates from high density-of-states points in a flat "f-like" band, which crosses the sp band along the $\Gamma\Lambda L$ direction (see Fig.

3). The lower energy peak of $E_f = 14.5$ eV is attributed to the minimum of this band at L_{4^-}, while the higher energy peak at $E_f = 16.0$ eV marks the maximum of this band near the gap induced by the interaction with the sp-like band (square box in Fig. 3), in analogy with band topologies calculated for Au (Ref. 5) and Pd.[4] Finally, for emission along the $\Gamma\Delta X$ direction, the flat f-like final band gives rise to weak structures at $E_f = 15.2$ and 17.6 eV [open diamonds ($\diamond$) and triangle (Δ) in Fig. 2, see also Fig. 5], which are attributed to the Γ_{6^-} critical point and the maximum of this band near the interaction region (square box in Fig. 3) with the sp-like final band along $\Gamma\Delta X$. All experimental conduction-band critical points at Γ, X, and L are summarized in Table I and Fig. 3 (solid dots). The uncertainties in these values are typically ± 0.5 eV.

The location of the sp-like final-band minima at X and L ($E_f = 10.5$ eV for X_{6^+} and $E_f = 7.6$ eV for L_{6^+}) is in good agreement with calculated *ab initio* RAPW values by Andersen[1] (10.6 and 7.37 eV, respectively; arrows in Fig. 3) and also with a semiempirical band-structure calculation by Smith.[3] In the latter calculation, an interpolation scheme has been used to calculate energy-band dispersions up to a final energy of ~ 14 eV above E_f (heavy solid lines in Fig. 3). To our knowledge, no band-structure calculation has been performed for Ir at higher energies such as for Pd (Ref. 4) and Au.[5] Therefore, final bands above $E_f = 13$ eV were constructed by using shifted and scaled theoretical Au bands for interpolation between the experimental critical points at Γ, X, and L.
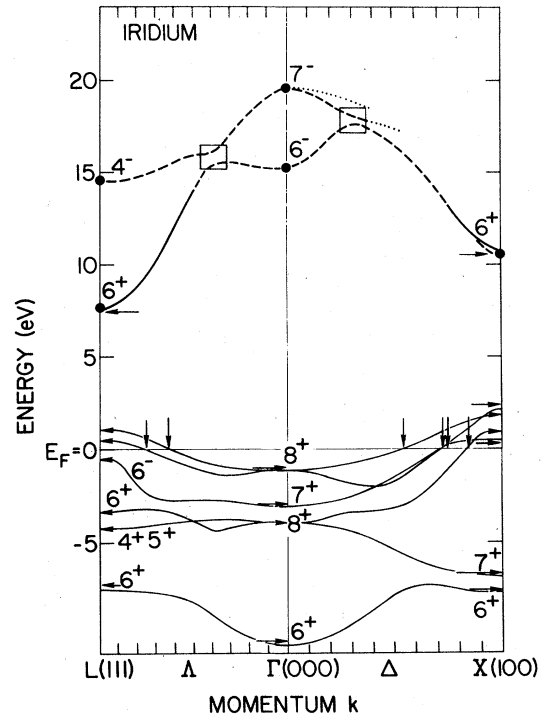
FIG. 3. Calculated valence bands after Arbman and Hörnfelt (Ref. 2) and semiempirical conduction bands along $\Gamma\Lambda L$ and $\Gamma\Delta X$. The solid dots at Γ, X, and L are experimentally determined conduction-band energies. Arrows denote RAPW energy levels and Fermi-level crossings calculated by Andersen (Ref. 1). Heavy solid lines denote conduction bands calculated by Smith (Ref. 3) using an interpolation scheme. Dashed lines denote our experimentally determined semiempirical bands (see Sec. III).

TABLE I. Experimental and theoretical energy levels for iridium at Γ, L, and X (eV relative to E_F).

Symmetry label	This work	Andersen (Ref. 1)	Arbman and Hörnfelt (Ref. 2)
Γ_{8^+}	-4.07 ± 0.08	-3.93	-4.03
Γ_{7^+}	-3.18 ± 0.08	-2.99	-3.11
Γ_{8^+}	-1.04 ± 0.05	-1.01	-1.09
Γ_{6^-}	$+15.2 \pm 0.5$		
Γ_{7^-}	$+19.5 \pm 0.5$		
$L_{4^+}L_{5^+}$	-4.25 ± 0.1	-4.23	-4.31
L_{6^+}	-3.35 ± 0.1	-3.29	-3.40
L_{6^-}	-1.0 ± 0.2	-0.54	-0.61
L_{6^+}	$+7.6 \pm 0.5$[a]	$+7.37$	
L_{4^-}	$+14.5 \pm 0.5$	$+7.37$	
X_{6^+}	$+10.5 \pm 0.5$	$+10.6$	

[a]An angle-integrated photoemission experiment (Ref. 29) reported $L_{6^+} = +7.1$ eV.

B. Valence-band energy dispersions

The semiempirical final-state bands described above have been used to determine E vs $\vec{k}$ energy dispersions of initial-state bands.[22] Energy uncertainties (for a given $k_\perp$) in the final bands are demagnified for the initial bands by the ratio of the slopes $\partial E/\partial k_\perp$) of the bands in question, typically by a factor of 5. This makes our method reasonably accurate for occupied bands. Typical uncertainties are less than ~ 0.1 eV and less than ~ 5–10% of the zone-boundary momentum, respectively. Calculated energy dispersions of initial bands[2] as well as Andersen's Fermi-level crossings and energy levels[1] at Γ, X, and L are shown in Fig. 3 for guidance in assignments of interband transitions. Double group symmetry labels at Γ, X, and L have been taken from Ref. 2.

The AREDC's from Ir(111) and Ir(100) (1×1) show dispersing peaks, labeled a, b, c, d, e, and f, which can be attributed to direct bulk interband transitions, as we discuss below.

Peak a shows a pronounced intensity maximum for $h\nu = 20.5$ eV at an initial energy $E_i = -1.04$ eV for both Ir(111) and Ir (100) normal emission. This peak is attributed to direct transitions from the upper d band to the free-electron-like sp-final band. For $h\nu = 20.5$ eV, this peak is degenerate in energy with the Γ_{7-} secondary electron structure (marked by $\blacklozenge$ in Fig. 2) which indicates that for this photon energy the transition takes place at the Γ point. This locates the Γ_{8+} point of the upper d band at $E_i = -1.04$ eV (Table I) and the Γ point of the sp-like conduction band (Γ_{7-} in Fig. 3) at a final energy of

$E_f = E_i + h\nu = 19.5$ eV. The enhancement of this transition a at Γ is stronger than just a superposition with the secondary electron structure, which indicates that there is a maximum in the transition amplitude. This also holds for some of the other critical points, as we will show.

Along the $\Gamma\Lambda L$ line, the peaks, labeled d and e in Fig. 1 disperse upwards with photon energy ($11.5 < h\nu < 17$ eV). These peaks are due to transitions from the lower spin-orbit split d bands into the lower energy part of the sp free-electron-like final band. At low photon energies ($h\nu \leq 14$ eV), features d and e just appear in the spectra; these transitions take place near the L point. The initial energies of these bands are $E_i = -3.35$ eV at the L_{6+} symmetry point and $E_i = -4.25$ eV at $L_{4+}L_{5+}$ (Table I). Thus the spin-orbit splitting of these initial bands at L is 0.91 eV. At photon energies between 18 and 20 eV, peaks d and e are nearly degenerate in energy with the double-peaked secondary electron structures at 14.5 and 16.0 eV above E_F and become enhanced. These spectral features correspond to transitions from the lower d bands into the flat f-like band along the $\Gamma\Lambda L$ line. For $h\nu > 20$ eV, the lower d bands disperse

weakly down again and couple to the free-electron-like final band near the Γ_{7-} point.

Emission from the lower d bands into two different final bands is also observed along the $\Gamma\Delta X$ line. Peaks d and e in Fig. 2 disperse strongly upwards as the photon energy increases from 17.5 to 21 eV. This is attributed to transitions into a region of the f-like band between Γ_{6-} and the "crossing point" with the "free-electron-like" band along $\Gamma\Delta X$. With increasing $h\nu$, peaks d and e vanish for $h\nu = 20$–21 eV and reappear for $22 \leq h\nu < 24$ eV; in the latter interval they disperse downwards again. The disappearance ($h\nu = 20$–21 eV) could be due to weak transitions into the small band-gap regions (square box in Fig. 3), induced by the interaction between both final bands along $\Gamma\Delta X$. At higher photon energies ($22 \leq h\nu \leq 24$ eV), the lower d bands again couple to the free-electron-like band. Thus the Γ points for the lower d bands appear twice in Fig. 2: spectral peaks d and e are degenerate in energy with the Γ_{6-} secondary electron structure at $h\nu = 18$ and 19 eV, respectively, and, once again with the Γ_{7-} secondary electron structure at $h\nu = 23$ and 24 eV, respectively. The latter degeneracy is also observed for emission along the $\Gamma\Lambda L$ line (Fig. 1). The initial energies for these enhanced transitions at Γ are -3.18 eV for Γ_{7+} and -4.07 eV for Γ_{8+}, the spin-orbit splitting being 0.89 eV (Table I).

Peak f, which is observed in normal emission from Ir(111), disperses downwards with increasing photon energy and joins the lower d bands at $h\nu \simeq 14$ eV. This feature is attributed to transitions from the sp-like valence band into the sp-like conduction band. At photon energies below 9.5 eV, for which this transition is expected to occur near the L point, peak f almost vanishes. By extrapolating the initial sp-like band towards the L point using a parabolic band shape, we locate the the L_{6-} critical point at the top of this band at $E_i = -1.0 \pm 0.2$ eV (Table I).

At low photon energies, the normal emission spectra from Ir(111) are dominated by peak ss, which rapidly decreases in intensity with increasing photon energy. This peak, which is located at an initial energy of -0.4 eV and does not disperse with photon energy, is sensitive to gas adsorption and lies in a sp-bulk band gap above the L_{6-} point at -1.0 eV. This feature is therefore attributed to emission from a sp-like surface resonance (centered at $\bar{\Gamma}$ of the surface Brillouin zone), which is similar to surface states observed for the noble metal (111) surfaces[24, 25] and the transition metal surfaces Ni(111) (Ref. 26) and Co(0001).[27]

Structures b and c, observed in normal emission from Ir(100) (1×1) (Fig. 2), disperse downwards for increasing photon energy. We attribute these features to transitions from the uppermost valence

bands to the sp free-electron-like final band. Due to the complexity of the band topology in this region of $\vec{k}$ space $(0.5\Gamma X < k_\perp < 0.8\Gamma X)$, we cannot unambiguously determine the $E(\vec{k})$ band dispersions in this region.

Finally, a nondispersive feature, labeled g in Fig. 2, is observed in the spectra of Ir(100) at $E_i = -2.75$ eV. It reaches maximum intensity at $h\nu \simeq 18$ eV and vanishes again at higher photon energies. The origin of this peak is not certain, it could be due to indirect transitions and reflects a high density-of-states critical point of the lower d bands at $k \simeq 0.5\Gamma L$ along the $\Gamma\Lambda L$ symmetry direction.

Energy versus momentum dispersions for the initial energy bands of Ir along $\Gamma\Lambda L$ and $\Gamma\Delta X$ are shown in Fig. 4. Experimental points were plotted using the data shown in Figs. 1 and 2 and the semi-empirical final bands discussed in Sec. III and shown in Fig. 3. The momentum k along $\Gamma\Lambda L$ and $\Gamma\Delta X$ is expressed in units of $k_{\text{BZ}}^{\langle 111\rangle}$ and $k_{\text{BZ}}^{\langle 100\rangle}$, respectively $(k_{\text{BZ}}^{\langle 111\rangle} = 1.42$ Å^{-1} is the distance between Γ and L, and $k_{\text{BZ}}^{\langle 100\rangle} = 1.64$ Å^{-1} is the distance between Γ and X).

It is interesting to note that for $0 < k/k_{\text{BZ}}^{\langle 100\rangle} < 0.3$ the dispersions of the lower d bands (e.g., spectral features d and e have been obtained from two different transitions, namely those to the f-like final band near Γ (solid dots in Fig. 4) and those to the free-electron-like final band near Γ (open dots). The close agreement using these two sets of data is evidence that the semiempirical final bands are constructed in a correct way.

If spin-orbit splitting is neglected, selection rules for normal emission along the Δ-symmetry line imply that only bands having Δ_5 symmetry are allowed for s-polarized radiation.[28] Although the spin-orbit splitting is appreciable for Ir, these selection rules are still approximately valid for rather isolated relativistic bands such as the low-lying Δ_1-like band joining Γ_{6+} and X_{6+} and the lower $\Delta_{2'}$-like band joining Γ_{8+} and X_{7+}. This accounts for the absence of transitions from these bands in our spectra for Ir(100). On the other hand, the upper d bands strongly intermix, since the spacing between neighboring bands is of the same order as the spin-orbit splitting. Therefore, the above "nonrelativistic" selection rules break down for these bands and they all show up quite strongly in our spectra.

Since normal emission spectra from Ir(111) have been obtained using mixed s-p polarized radiation, all initial bands are allowed along the Λ direction. In spite of this, the lowest lying Λ-like band is not seen in the spectra. This is presumably due to the fact that this level has a small ionization cross section for our range of photon energies, as is the case for Cu.

IV. DISCUSSION OF THEORY AND EXPERIMENT

The RAPW energy eigenvalues at Γ, L, and X calculated by Andersen[1] (Table I, arrows in Fig. 4) generally agree within 0.2 eV with our experimental values. A notable exception is the L_{6-} symmetry point for which the calculated binding energy is ~ 0.4 eV larger than measured. The L_{6-} point corresponds to the $L_{2'}$ point for nonrelativistic metals such as Ni and Cu and has sp-like symmetry. Similar results have been obtained for Ni (Ref. 11) and Co,[27] for which measured $L_{2'}$ critical points are lower in binding energy that calculated values. The calculated locations of the spin-orbit split lower d bands at L $(L_{4+}+L_{5+}$ and $L_{6+})$ agree within 60 meV with the measured positions. The spin-orbit splitting $L_3 \rightarrow L_{4+} + L_{5+} + L_{6+}$ was measured to be 0.90 ± 0.05 eV to be compared with Anderson's value of 0.94 eV. At Γ, these bands are split into $\Gamma_{25'} \rightarrow \Gamma_{7+} + \Gamma_{8+}$ by 0.89 ± 0.05 eV (0.94 eV calculated).

Energy dispersions of initial bands along $\Gamma\Lambda L$ and $\Gamma\Delta X$ have been calculated by Arbman and Hörnfelt[2] and are shown in Figs. 3 and 4 (solid lines). This RAPW-type calculation is similar to that by Andersen, the difference being that a $5d^8 6s$ atomic configuration was used instead of a $5d^7 6s^2$ configuration for the starting potential. Energy values at Γ, X, and L differ from Andersen's value by less than 0.1 eV and are in slightly better agreement with experiment at Γ (Table I). Most of the differences between experi-

FIG. 4. Experimental E vs $\vec{k}$ energy-band dispersions for Ir along $\Gamma\Lambda L$ and $\Gamma\Delta X$. Bands are labeled a, b, c, etc., using the notation of Figs. 1 and 2. Solid (open) dots are transitions to the first (second) final bands, in order of their energy. Arrows denote energy levels and Fermi-level crossings after Andersen (Ref. 1). Solid lines denote calculated bands after Arbman and Hörnfelt (Ref. 2).

ment and theory occur in the actual shape of the bands. In particular features b and c along the $\Gamma\Delta X$ direction do not follow the theoretical band dispersions. However, the location of the Fermi level crossing of b is in good agreement with Andersen's model of the Fermi surface and with de Haas–van Alphen data.[9] The Fermi-level crossing for feature c, which determines the size of the small "$X3$" hole pocket[1] near X, cannot accurately be determined from our data; however, our limited results seem to be consistent with de Haas–van Alphen data.[8] Fermi-level crossings given by our $E(\vec{k})$ dispersions (Fig. 4) for the other bands (which give rise to closed electron surfaces centered at Γ) are in agreement with both calculations and with Fermi-surface data.[9]

For most of the empty conduction-band critical points, theoretical calculations are not available to compare with our experimental results. The only calculated values for the sp-conduction band minima at L_{6+} and X_{6+} agree with our results within the ± 0.5 eV error of the measurement (Table I). The L_{6+} critical point obtained by Traum and Smith[29] from angle-integrated photoemission data for clean and cesiated polycrystalline samples is 0.5 eV lower than our value (Table I).

Some interband transitions show $h\nu$-dependent intensity maxima, or "resonances," at certain photon energies. We note a particularly strong transition from the upper d band into the free-electron-like final band, which takes place at the Γ point $(\Gamma_{8+}\rightarrow\Gamma_{7-})$. No transition was observed from this band into the lower final band near $\Gamma(\Gamma_{8+}\rightarrow\Gamma_{6-})$. Transitions from the lower d bands show large transition matrix elements for several transitions, i.e., for $\Gamma_{7+},\ \Gamma_{8+}\rightarrow\Gamma_{6-}$ and $\Gamma_{7+},\ \Gamma_{8+}\rightarrow\Gamma_{7-}$. The sharpest $h\nu$-dependent transition is seen for normal emission along the $\Gamma\Lambda L$ line near the crossing point between the two final bands at $k\simeq0.4\Gamma L$. These resonances have also been observed for Au (Ref. 30) and Pd.[12] The intensity of transitions from the lower spin-orbit split d bands into the bottom of the free-electron-like final band becomes very small near the L point. This can be explained by the fact that the initial states are predominantly d like, whereas the final state is mainly s like. These transitions would therefore be forbidden according to atomic dipole selection rules.[31]

V. PHOTOEMISSION FROM Ir(100) (5 × 1)

The most stable structure for the clean Ir(100) surface is the (5 × 1)-reconstructed surface phase. This surface structure is routinely obtained after cleaning and subsequent annealing, and in this respect Ir(100) is similar to the Pt(100) and Au(100) surfaces. These surfaces have been interpreted as consisting of a single hexagonal close-packed overlayer on top of a

(100) substrate, with six rows of surface atoms being commensurate with five rows of substrate atoms.[32–34] It might therefore be expected that the (5 × 1) reconstruction induces strong surface umklapp scattering of the outgoing photoelectrons.

Normal emission spectra for the (5 × 1) surface are shown in Fig. 5. Upon comparison with the spectra from Ir(100) (1 × 1) in Fig. 2, it is seen that the strong $h\nu$-dependent resonances, observed for the
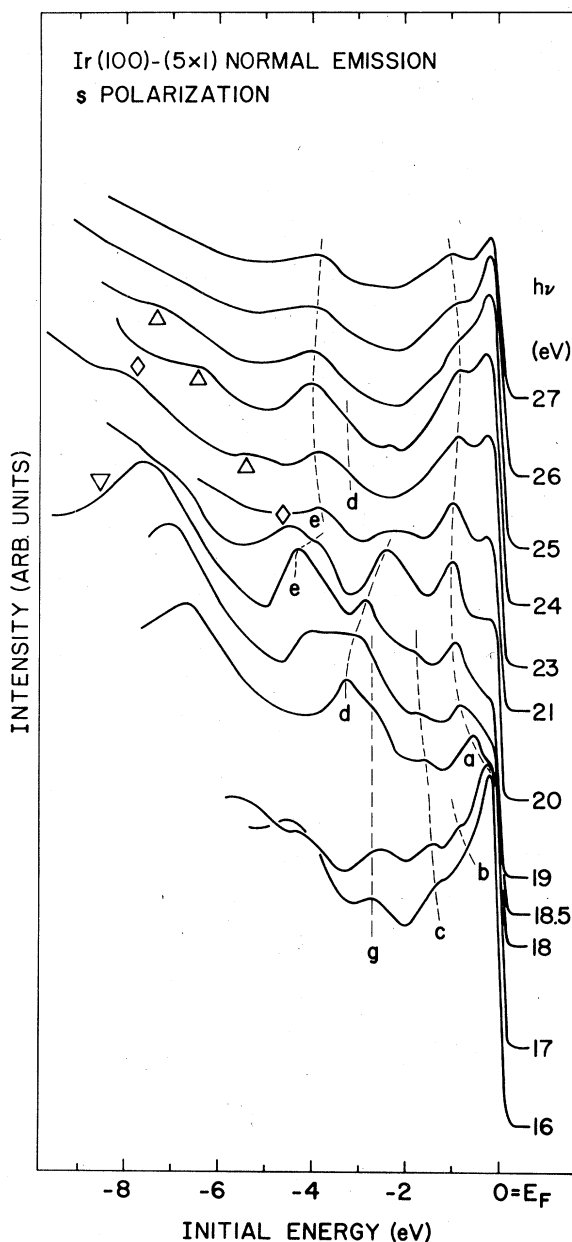
FIG. 5. Normal emission AREDC's from Ir(100) (5 × 1). Symbols are as in Figs. 1 and 2.

(1×1) surface are considerably weakened for the (5×1) reconstructed surface. Surface umklapp scattering redistributes the bulk interband emission intensities in $\vec{k}$ space. For example, the intense interband transition $\Gamma_{8+} \rightarrow \Gamma_{7-}$ observed for the (1×1) face at $E_i = -1.04$ eV and $h\nu = 21$ eV becomes ~ 6 times weaker in intensity for the (5×1) face because photoelectrons are scattered away from the normal direction. The same effect is observed for the interband transitions $\Gamma_{8+} \rightarrow \Gamma_{7-}$ and $\Gamma_{7+} \rightarrow \Gamma_{7-}$ at $E_i = -4.07$ and -3.18 eV, respectively. Energy dispersions for these structures were found to be identical for both the (1×1) and (5×1) surfaces.

These results show that surface reconstruction as observed for Ir significantly affects the intensities of bulk interband transitions, thereby complicating the interpretation of photoemission spectra in terms of bulk band structure.

VI. CONCLUSIONS

Angle-resolved photoemission spectra for Ir(100) and Ir(111) have been measured for photon energies $8 \leq h\nu \leq 30$ eV and used to determine the energy dispersions of $E(\vec{k})$ electronic bands along the $\Gamma\Lambda L$ and $\Gamma\Delta X$ directions. RAPW calculations by Andersen and Arbman and Hörnfelt have been compared with these results; these calculated eigenvalues at high-symmetry points generally show good agreement with experiment, with errors ranging from ~ 0 to 0.2

eV for the valence bands. One exception is the position of the sp-like L_{6-} point which is calculated to be ~ 0.4 eV above the measured L_{6-} point at -1.0 eV.

At certain photon energies, the interband transition intensities are strongly enhanced. The lower d band has a large resonance for transitions into the flat f-like final band, whereas the upper d band dominates for transitions into the free-electron-like final band.

An assignment of bulk interband transitions for normal emission from Ir(100) has been greatly facilitated by taking data for a specially prepared unreconstructed metastable Ir(100) (1×1) surface. The stable (5×1) reconstructed Ir(100) surface gives rise to strong surface umklapp scattering, to the extent that the above resonancelike features are significantly smeared out in $\vec{k}$ space. The same effect is likely to occur for photoemission from the (5×20) reconstructed Pt(100) and Au(100) surfaces. As for Ir(100), these surfaces can also be prepared in a metastable (1×1) phase, which should also be very useful for determining the electronic structure of Pt and Au using their (100) surfaces.

ACKNOWLEDGMENTS

[1]O. K. Andersen, Phys. Rev. B **2**, 883 (1970).
[2]G. O. Arbman and S. Hörnfelt, J. Phys. B **2**, 1033 (1972).
[3]N. V. Smith, Phys. Rev. B **9**, 1365 (1974).
[4]N. E. Christensen, Phys. Rev. B **14**, 3446 (1976).
[5]N. E. Christensen, Phys. Rev. B **13**, 2698 (1976).
[6]J. H. Weaver, Phys. Rev. B **11**, 1416 (1975).
[7]J. H. Weaver, C. G. Olson, and D. W. Lynch, Phys. Rev. B **15**, 4115 (1977).
[8]J. J. Grodski and A. E. Dixon, Solid State Commun. **7**, 735 (1969).
[9]S. P. Hörnfelt, L. R. Windmiller, and J. B. Ketterson, Phys. Rev. B **7**, 4349 (1973).
[10]U. Gerhardt and E. Dietz, Phys. Rev Lett. **26**, 1477 (1971).
[11]F. J. Himpsel, J. A. Knapp, and D. E. Eastman, Phys. Rev. B **19**, 2919 (1979).
[12]F. J. Himpsel and D. E. Eastman, Phys. Rev. B **18**, 5236 (1978).
[13]G. V. Hansson and S. A. Flodström, Phys. Rev. B **18**, 1572 (1978).
[14]H. Thomas, Z. Phys. **147**, 395 (1957); H. Mayer and H. Thomas, *ibid.* **147**, 419 (1957); S. Methfessel, *ibid.* **147**, 422 (1957).
[15]J. F. van der Veen, F. J. Himpsel, and D. E. Eastman, Solid State Commun. **34**, 33 (1980).
[16]T. N. Rhodin and G. Broden, Surf. Sci. **60**, 466 (1976).
[17]H. P. Bonzel, C. R. Helms, and S. Kelemen, Phys. Rev. Lett. **35**, 1237 (1975).
[18]J. F. Wendelken and D. M. Zehner, Surf. Sci. **71**, 178 (1978).

[19]D. E. Eastman, J. J. Donelon, N. C. Hien, and F. J. Himpsel, Nucl. Instrum. Methods **172**, 327 (1980).
[20]P. R. Norton, J. Catal. **36**, 211 (1975).
[21]C. R. Helms, H. P. Bonzel, and S. Kelemen, J. Chem. Phys. **65**, 1773 (1976).
[22]B. Feuerbacher and N. E. Christensen, Phys. Rev. B **10**, 2373 (1974).
[23]N. E. Christensen and B. O. Seraphin, Phys. Rev. B **4**, 3321 (1971).
[24]P. O. Gartland and B. J. Slagsvold, Phys. Rev. B **12**, 4047 (1975).
[25]P. Heimann, H. Neddermeyer, and H. F. Roloff, J. Phys. C **10**, L17 (1977).
[26]F. J. Himpsel and D. E. Eastman, Phys. Rev. Lett. **41**, 507 (1978).
[27]F. J. Himpsel and D. E. Eastman, Phys. Rev. B **20**, 3217 (1979).
[28]J. Hermanson, Solid State Commun. **22**, 9 (1977).
[29]M. M. Traum and N. V. Smith, Phys. Rev. B **9**, 1353(1974).
[30]J. Hermanson, J. Anderson, and G. Lapeyre, Phys. Rev. B **12**, 5410 (1975).
[31]N. V. Smith, Phys. Rev. B **19**, 5019 (1979).
[32]P. W. Palmberg and T. N. Rhodin, Phys. Rev. **161**, 586 (1967).
[33]A. Ignatiev, A. V. Jones, and T. N. Rhodin, Surf. Sci. **30**, 573 (1972).
[34]J. F. van der Veen, F. J. Himpsel, and D. E. Eastman, Phys. Rev. Lett. **44**, 189 (1980).